



Origin and mechanical significance of foliated cataclastic rocks in the cores of crustal-scale faults: Examples from the Median Tectonic Line, Japan

S. P. Jefferies,¹ R. E. Holdsworth,¹ T. Shimamoto,² H. Takagi,³ G. E. Lloyd,⁴ and C. J. Spiers⁵

Received 5 December 2005; revised 20 July 2006; accepted 29 August 2006; published 15 December 2006.

[1] The Median Tectonic Line (MTL) is Japan's largest onshore fault and has been active since the mid-Cretaceous. Foliated cataclastic fault rocks are exceptionally well exposed in the fault core at Anko, Nagano Prefecture. Following an early phase of mylonitization and exhumation during left-lateral shearing, brittle fracture and cataclasis occurred leading to the development of centimeter- to submillimeter-spaced, fault zone parallel fracture systems. These fracture systems established an initial architectural hierarchy that influenced the subsequent development of foliated cataclasites and gouge. Initially, fracture systems coalesced to form interconnected zones of fine-grained ultracataclasite. Fluid influx at the onset of grain-scale brittle deformation led to precipitation of fibrous chlorite within the ultracataclasites, ultimately leading to the development of an interconnected network of foliated, phyllosilicate-rich cataclasites and gouges in the core of the MTL. The brittle reduction of grain size and ingress of a chemically active fluid phase simultaneously promoted reaction softening and diffusive mass transfer in the foliated ultracataclasites, leading to rate-dependent "frictional-viscous" flow at sub-Byerlee friction values. Associated weakening is indicated by the preferential localization of deformation within the ultracataclasites. A protracted sequence of carbonate mineralization and cementation events is also recognized during the fault rock evolution and suggests episodic periods of fluid overpressuring. A crustal-scale fault zone model is proposed, suggesting that the foliated cataclasites/gouges are weak in the long term and represent shallower crustal equivalents of phyllonitic fault rocks exposed in more deeply exhumed fault zones, including other parts of the MTL.

Citation: Jefferies, S. P., R. E. Holdsworth, T. Shimamoto, H. Takagi, G. E. Lloyd, and C. J. Spiers (2006), Origin and mechanical significance of foliated cataclastic rocks in the cores of crustal-scale faults: Examples from the Median Tectonic Line, Japan, *J. Geophys. Res.*, *111*, B12303, doi:10.1029/2005JB004205.

1. Introduction

[2] It is widely believed that reactivated crustal-scale fault zones are weak relative to adjacent regions of intact rock. Such fault zones often contain exhumed fault rock suites with textures that preserve valuable information about the deformation mechanisms operating at depth in both ancient and modern settings [e.g., *Sibson, 1977; Schmid and Handy, 1991; Holdsworth et al., 2001*]. Recent field-based research along major faults [e.g., *Imber et al., 2001; Stewart et al.,*

2000; Gueydan et al., 2003; Collettini and Holdsworth, 2004; Wibberley, 2005] has focused on the importance of foliated, fine-grained phyllosilicate-rich fault rocks, or phyllonites, formed close to the main load-bearing region of the crust at the frictional-viscous transition (i.e., 8–15 km depths). The textural sequences preserved in these rocks are similar to those developed during analogue deformation experiments on fine-grained "fault rocks" [e.g., *Bos and Spiers, 2000, 2002; Bos et al., 2000a, 2000b*]. These experimental results predict a profound and long-term weakening of faults that develop phyllonites and provide explanations for reactivated faults, low-angle normal faults and anomalously weak, plate boundary structures [*Holdsworth, 2004*].

[3] Foliated brittle fault rocks have been recognized along many major crustal discontinuities [e.g., *Chester et al., 1985, 1993; Chester and Logan, 1986*] and are generally thought to have formed at $\ll 10$ km depth. They have been reproduced also experimentally [e.g., *Yund et al., 1990; Beeler et al., 1996*]. The rheological significance of such foliated brittle fault rocks is rather poorly understood,

¹Reactivation Research Group, Department of Earth Sciences, University of Durham, Durham, England, UK.

²Department of Geology and Mineralogy, Graduate School of Science, Kyoto University, Kyoto, Japan.

³Department of Earth Science, Waseda University, Shinjuku, Tokyo, Japan.

⁴Department of Earth Sciences, University of Leeds, Leeds, UK.

⁵HPT Laboratory, Department of Earth Sciences, Utrecht University, Utrecht, Netherlands.

although they are thought to be associated with fault zone weakening [e.g., *Chester*, 1995] with evidence for both grain-scale reaction softening and the operation of fluid-assisted diffusional mechanisms in many cases [e.g., *Evans and Chester*, 1995]. The present study focuses on the development of foliated cataclasite and gouge along the Median Tectonic Line (MTL), Nagano Prefecture, SW Japan (Figure 1a). The development of the foliated cataclasites is compared with that of phyllonites from a more deeply exhumed section of the MTL and with expectations based on a recent, crustal-scale, fault strength model. The comparison is used to discuss the implications for fault zone rheology and to test the hypothesis that the foliated cataclastic rocks at Nagano are shallower crustal equivalents of the phyllonitic sequences recognized elsewhere along the MTL.

2. Geological and Structural Setting

[4] The MTL is a major crustal-scale fault with a strike length of >1000 km and a displacement history originating in the early Cretaceous. Displacement estimates are poorly constrained, ranging from 200 to 1000 km [*Ichikawa*, 1980]. Today, the MTL has a steep to subvertical dip and forms the boundary between the low-P/high-T Ryoke metamorphic belt of granitoids and metasedimentary rocks to the north and the high-P/low-T Sambagawa belt of accretionary complex metasedimentary rocks to the south (Figure 1a). The fault zone displays a wide variety of fault rocks generated at different levels in the midcrust to upper crust, now exhumed as a consequence of continued activity, uplift and fault reactivation.

[5] Within the Ryoke Belt (Figure 1a), a broad (up to 5 km wide) zone of mylonitization formed during sinistral top-to-south shearing in the late Cretaceous to earliest Tertiary [*Ito*, 1978] when the MTL was a shallowly inclined structure. A later and narrower central or “core” region of sinistral strike-slip displacements formed during the early Tertiary on a steeply dipping MTL [e.g., *Ichikawa*, 1980; *Hara et al.*, 1980; *Ohtomo*, 1993]. This deformation becomes increasingly brittle, with the development of foliated cataclasites, breccias and gouges, as the fault core is approached [e.g., *Takagi*, 1984, 1986; *Wibberley and Shimamoto*, 2003; *Jefferies et al.*, 2006]. A subsequent dextral strike-slip reactivation, with displacements localized within incohesive and phyllosilicate-rich fault rocks typically found within 10 m of the central slip zone, is recognized on the southwestern parts of the MTL [e.g., *Okada*, 1980; *Wibberley and Shimamoto*, 2003; *Jefferies et al.*, 2006].

[6] In Nagano Prefecture, the MTL runs approximately N-S with a subvertical dip (Figures 1a and 2a) and is cut out to the north by the Itoigawa-Shizuoka Tectonic Line (ISTL) [*Takagi*, 1986]. The present paper focuses on fault rocks derived from the Ryoke belt, which comprises amphibolite-facies psammitic and pelitic schists, with variable mica content, and subordinate units of tonalitic orthogneiss [*Ohtomo*, 1993; *Yamamoto*, 1994]. These rocks characteristically contain white mica, biotite, quartz, plagioclase, garnet, sillimanite and andalusite [*Yamamoto*, 1994]. A mid-Cretaceous (circa 100 Ma) age estimate for this regional metamorphism has been suggested using radiomet-

ric age data and geological evidence [*Suzuki and Adachi*, 1998]. The Sambagawa belt in Nagano Prefecture is composed mainly of greenschist facies pelites and minor basic schists [*Takagi*, 1986].

[7] The Hiji tonalitic gneiss body in the Nagano Prefecture is the oldest of the granitic rocks in the Ryoke Belt with a mid-Cretaceous (circa 95 Ma) age of emplacement [*Suzuki and Adachi*, 1998]. It consists of quartz, plagioclase, K-feldspar, biotite and hornblende in varying proportions and toward the center of the body develops a gneissose banding trending subparallel (010°–040°) to the MTL with steeply west dipping to subvertical orientations [*Takagi*, 1986]. Adjacent to the MTL, the tonalitic gneiss has been deformed into a zone of subvertical mylonites up to 1 km wide with ubiquitous sinistral shear criteria [*Takagi*, 1984, 1986]. The effects of brittle sinistral deformation are localized in the fault core region, within which cataclastic rocks, many of them foliated, are derived from the mylonites as subvertical intercalated belts locally up to 200 m wide.

[8] The present study was carried out on a ~240 m NE-SW section of the MTL fault core well exposed by a tributary of the Aokigawa River in the Anko region (Figures 1 and 2) [*Tanaka et al.*, 1996]. The boundary between the (often foliated) Ryoke-derived cataclastic rocks in the fault core and the Ryoke-derived mylonites that lie to the west is not exposed. The Sambagawa rocks along this section comprise generally poorly exposed black (pelitic) and green (basic) schists [*Takagi*, 1986; *Tanaka et al.*, 1996] and are not discussed in this paper.

3. MTL Fault Core, Anko Section

3.1. Field Relationships and Mesostructures

3.1.1. Faults

[9] The Anko section is cut by at least two generations of mesoscale faults that appear to postdate all other structures, including foliated cataclasites in the fault core. The earlier fault set are more significant in terms of displacement as they intercalate fault rocks derived from both Ryoke and Sambagawa protoliths in a 20–30 m wide central region of the fault core (Figures 1b, 2a, and 3a). These faults strike N-S at low angles to the MTL, with steep dips and shallowly plunging slickenlines consistent with strike-slip movements (Figures 1c and 2, left). No unambiguous senses of shear could be determined where slickenlines are preserved in exposed fault surfaces. Associated with many of these late brittle faults is a zone of hydrothermal alteration up to 1 m wide where the fault rocks exhibit a “bleached” appearance. Narrow (<10 cm wide) carbonate-cemented, unfoliated gouges are developed along these faults (Figure 3b) together with late Fe-staining and pyrite mineralization. A later generation of moderately dipping reverse faults trending ENE and dipping south (Figure 2b, left), crosscut all other structures [see *Tanaka et al.*, 1996] and are associated with minor sulphide mineralization.

3.1.2. Ryoke Mylonites

[10] Mylonitized Ryoke psammitic and pelitic rocks crop out toward the southwestern end of the Anko section, intersliced with units of foliated quartzo-feldspathic cataclasite (Figure 1b). They are fine grained (~0.05–0.1 mm) and commonly exhibit a distinctive orange and black

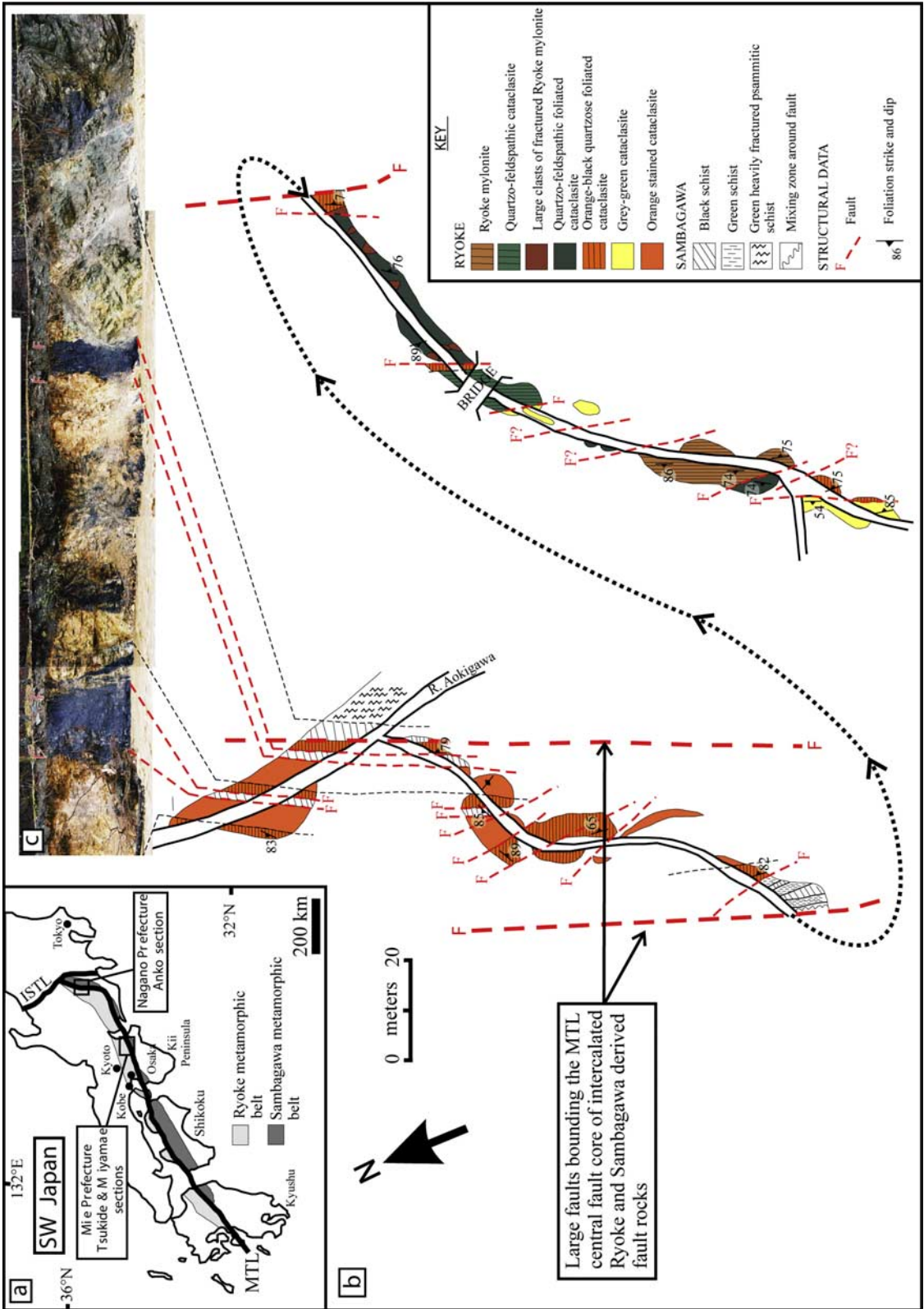


Figure 1. (a) Median Tectonic Line (MTL), SW Japan, showing adjacent metamorphic belts. ISTL = Itoigawa-Shizuoka Tectonic Line. (b) Simplified geological map of Anko section of MTL fault core [after Tanaka *et al.*, 1996]. (c) Photograph of a section of fault core, looking NE.

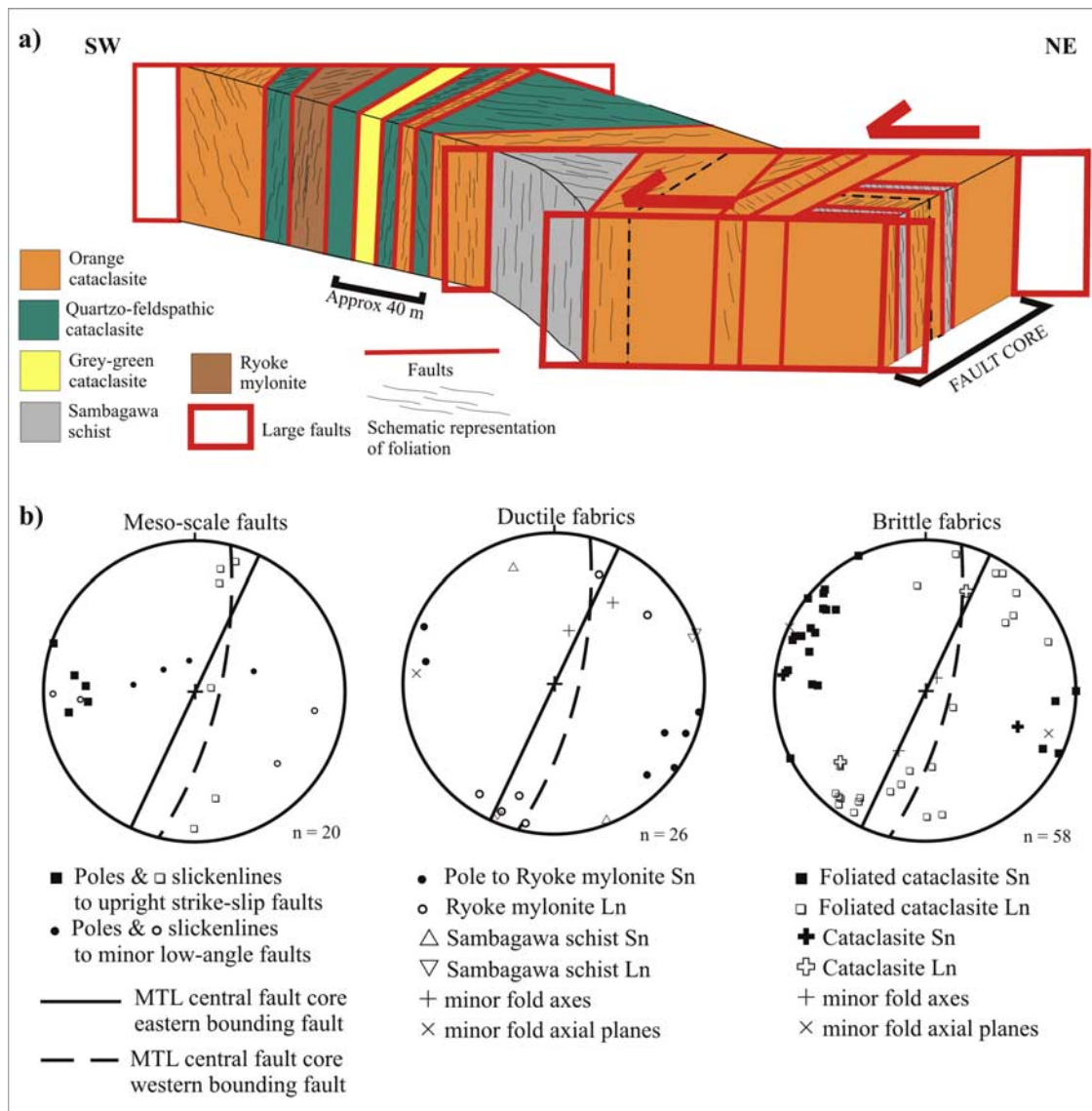


Figure 2. (a) Schematic three-dimensional sketch of MTL section shown in Figure 1a showing fault and foliation geometries in region west of the River Aokigawa. (b) Stereograms of structural data on (left) faults, (middle) ductile deformation fabrics, and (right) brittle deformation fabrics, respectively (Sn, foliation; Ln, mineral lineation).

banded appearance due to Fe staining of the more quartzo-feldspathic psammitic layers (Figure 3c) and very fine grained (<0.05 mm) black micaceous pelitic layers, respectively. The interbanding of orange and black units is developed on tens of centimeter- to submillimeter scales and appears to be a relict compositional layering transposed almost entirely into concordance with the strong mylonitic foliation (Figure 3c). The foliation has a uniform orientation (mean 019/78W) with a mineral lineation defined by mica and elongated quartz plunging shallowly toward either the NNE or SSW (Figure 2b, middle). Intrafolial isoclinal folds are locally present, but few hinge lines actually exposed. Where they can be measured, fold hinges are upright with shallow to moderate NNE plunges (Figure 2b, middle). These folds appear to have formed during intense ductile shearing associated with mylonitization. Late calcite

veins, <1 cm wide, occur also and crosscut the mylonite fabric.

3.1.3. Quartzo-Feldspathic Cataclasite

[11] The quartzo-feldspathic cataclasite crops out in a ~10 m wide zone (Figure 1b) and is derived from Ryoke tonalitic mylonite. Few original features are visible due to pervasive grain-scale crushing, but the rock is composed of a mixture of protocataclasite and variably foliated ultracataclasite (Figure 3d). In the protocataclasite sections, feldspar grains reach up to ~1.2 mm and in isolated regions, the relict mylonitic foliation remains visible. The ultracataclasites are dark gray-black and individual grains are undistinguishable.

3.1.4. Quartzo-Feldspathic Foliated Cataclasite With Clasts of Fractured Mylonite

[12] This fault rock is continually exposed in a 40 m long section west of the central fault core (Figure 1b). It is

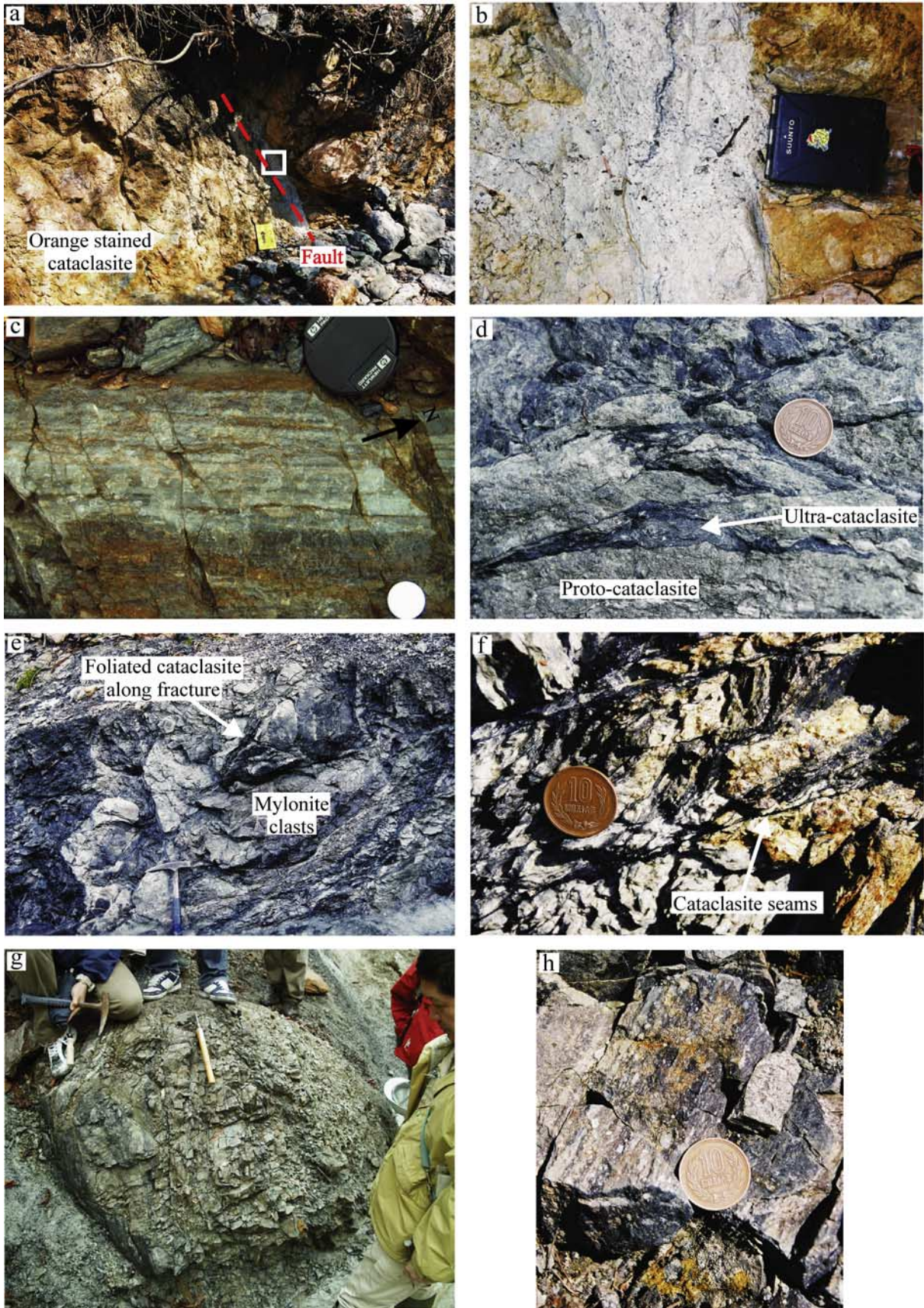


Figure 3

mineralogically similar, but finer grained, to the quartzo-feldspathic cataclasite and has suffered more intense deformation. Regions of light gray cataclasite derived from fractured quartzo-feldspathic mylonite are recognizable, surrounded by dark gray foliated ultracataclasite (Figures 3e and 3g). Finer-grained regions display a crude mesoscopic foliation defined by the preferential alignment of an anastomosing and coalescing network of fracture surfaces with centimeter- to submillimeter spacing (Figures 3e–3f). A weak to moderately strong ultrafine foliation oriented subparallel to the fracture foliation is developed also. Collectively, the foliations strike approximately NNE-SSW with a steep to vertical dip. A fine mineral lineation, defined by aligned chlorite grains, plunges gently to moderately NNE or SSW (Figure 2b, right). Clasts in the less deformed light gray cataclasites reach up to ~1 mm, while individual grains in the ultracataclasites often cannot be distinguished. Thin (millimeter to submillimeter) seams of ultracataclasite lie along many fracture surfaces that define the mesoscale foliation (Figure 3f), and also locally form crosscutting veins (Figure 3e) consistent with injection of mobilized material into voids during deformation. Open to tight centimeter-scale folds are present locally in sections where the mesoscopic foliation is most intensely developed, which suggests that foliation development is associated with the onset of mesoscopic cataclastic flow, although no consistent hinge orientation or sense of vergence is preserved in the available exposures.

[13] Lenticular clasts of relict gray mylonitic tonalite up to 3 m across and 5 m long are widely preserved and are wrapped by the cataclasite foliation (Figures 1b, 3e, and 3g). They are internally disrupted by networks of brittle fractures, some of which are associated with well-developed seams of foliated ultracataclasite up to 10 cm wide. Within the center of some larger tonalitic clasts, cataclasis is limited and good mylonitic textures are preserved (Figure 3h). Elongate feldspar porphyroclasts up to 5 mm long are aligned parallel to the mylonitic foliation in the fine-grained quartz-mica matrix. A compositional layering defined by alternating quartz-rich and quartz-poor bands lies parallel to the mylonitic foliation. Toward the edges of the large clasts, the intensity of cataclasis increases and mylonitic textures are progressively obliterated.

3.1.5. Orange-Black Quartzose Foliated Cataclasite and Gouge

[14] This very distinctive unit crops out mainly in the central region of the fault core where it is intercalated with orange-stained cataclasite and units derived from Sambagawa schists (Figure 1b). The meter to submillimeter interbanding of orange and black units (Figures 1c and 4a) appears to resemble the Ryoike psammitic and pelitic mylonites that outcrop upstream (Figure 4a), but the coarser (up to ~1 mm) grained bands of Fe-oxide-stained orange

cataclasite contain no visible feldspar and appear to be composed almost entirely of quartz and subordinate carbonate. The black bands form a closely spaced, anastomosing and coalescing network of extremely fine grained foliated ultracataclasites (Figure 4b), although the textures and mineralogy cannot be resolved in the field. The foliation is consistently steeply dipping to subvertical, but varies in strike from N-S to NE-SW. An associated mineral lineation defined by aligned chlorite grains plunges shallowly to moderately S-SW or N-NE (Figure 2b, right). The variations in strike appear to reflect the development of sinistral shear band structures on centimeter to meter scales, with regions of NE-SW trending foliation having undergone small clockwise back rotation between N-S trending higher strain zones (e.g., see Figure 4c).

[15] Field evidence suggests that the formation of the dark ultracataclasite localizes along fractures with cm to submillimeter spacing (Figure 4b). The foliation is defined by the parallel alignment of grains and a dense, closely spaced fracture network. The dark seams and associated fractures crosscut the orange quartzose layers and clasts and appear to break them down from the edges inward to form typically elongate quartz clasts that appear to be being smeared within the foliation due to the effects of cataclastic flow (Figure 4b). Injection seams of dark ultracataclasite cutting across orange quartzose cataclasites are common and are locally folded and flattened parallel to the foliation (Figure 4d).

[16] Centimeter-scale Riedel-type shears, coated with dark ultracataclasites, are widely developed and lie anticlockwise at angles of up to ~45° to the crude foliation, consistent with sinistral shear (Figure 4b). Locally, the shears and foliated dark ultracataclasite are folded by irregular centimeter-scale open to tight folds (Figure 4e) with variable orientations.

[17] The orange black quartzose foliated cataclasite appear to lose coherency to form gouges with a pervasive flow foliation adjacent to intercalated units of other fault rock types (Figures 4c, 4f, and 4g). Relict clasts of quartzose cataclasite and pale carbonate up to 10 cm across are locally preserved strongly wrapped by the foliation. The wrapping is often slightly asymmetric and, together with the local development of centimeter-spaced shear bands oriented anticlockwise to the foliation, suggest a sinistral shear sense (Figures 4b, 4f, and 4g). The foliation is locally folded by centimeter-scale tight to isoclinal folds with mainly subvertical plunges that most likely formed due to strike-slip shearing, although a consistent sense of vergence could not be ascertained. Fold hinges are often thickened, with pinching and shearing out of fold limbs by fractures and associated ultracataclasite seams.

[18] The highly foliated gouges characteristically preserve interlinked vein networks of white and orange car-

Figure 3. (a) Section view, looking north, of bleached carbonate rich gouge adjacent to fault cutting through orange stained cataclasite. Box shown location of Figure 3b. (b) Close-up of gouge along fault shown in Figure 3a. (c) Plan view of Ryoike mylonite derived from psammitic. (d) Section view of quartzo-feldspathic cataclasite showing ultracataclasite seams developing along fractures. (e) Section view of tonalitic mylonite clasts within cataclasite. (f) Section view of ultracataclasite injection along fractures through quartzo-feldspathic foliated cataclasite. (g) View, looking north, of large meter-scale tonalitic mylonite clast. (e) Close up plan view of tonalitic mylonite in clast.

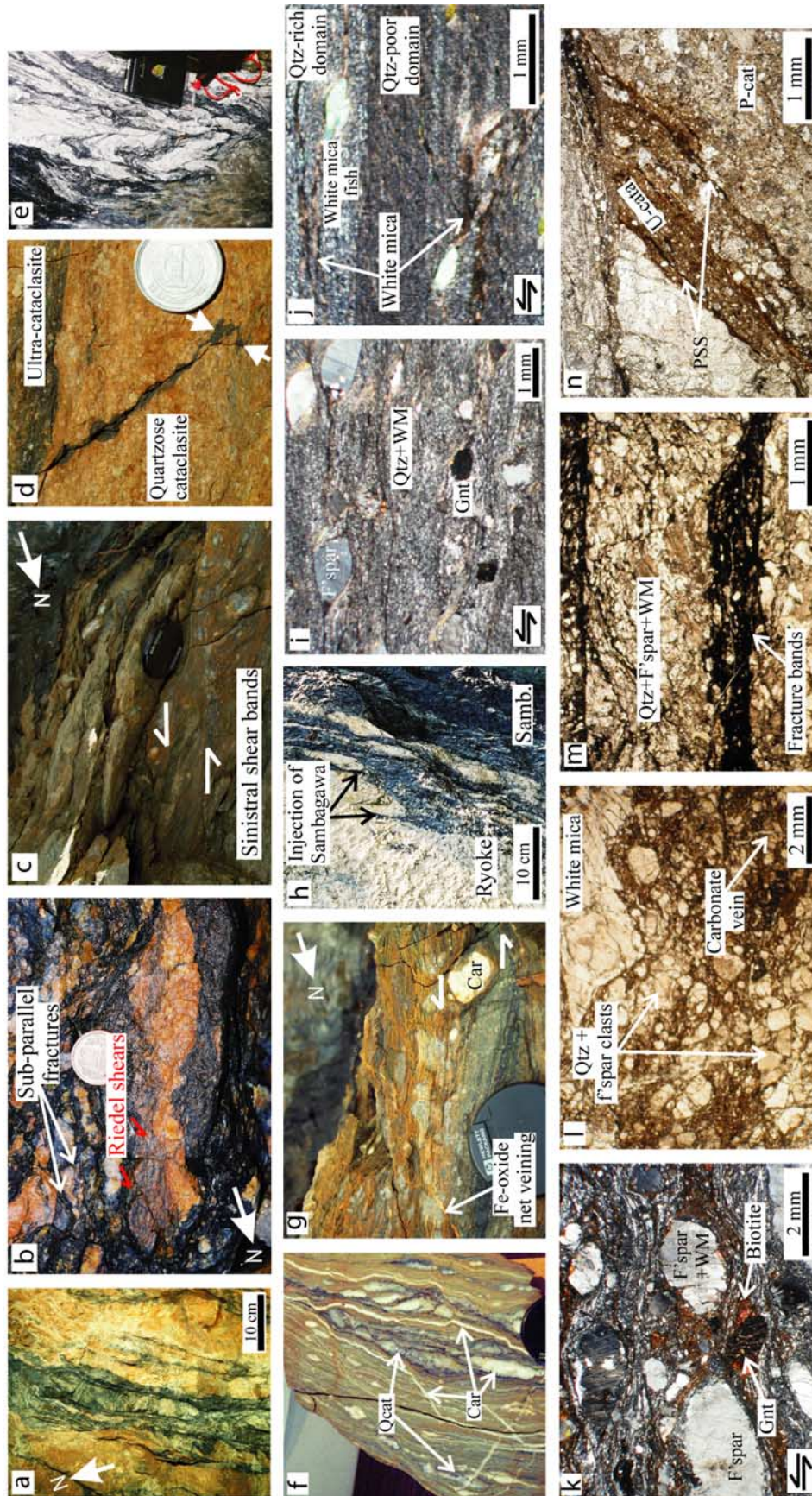


Figure 4

bonate and Fe-oxide, with individual veins typically less than 1mm wide. The veins anastomose and coalesce and are preferentially aligned subparallel to the foliation, although they locally crosscut and therefore postdate this fabric (Figures 4f–4g). Regions of foliated gouge adjacent to orange Ryoke-Sambagawa contacts appear to have been particularly incohesive, with evidence of cusped-lobate boundaries between units of Ryoke- and Sambagawa-derived gouge. In some localities, black Sambagawa-derived gouge appears to have been injected into orange Ryoke-derived units (Figure 4h).

3.1.6. Gray-Green and Orange-Stained Cataclasites

[19] Both these fault rocks units are essentially unfoliated. The pale gray-green cataclasite crops out in two fault-bounded slices (Figures 1b and 2a). It appears to be derived from a Ryoke quartzo-feldspathic mylonite as mylonitic foliation and feldspar porphyroclasts up to 0.6 mm across remain visible. A few weakly foliated and extremely fine grained ultracataclasite bands have formed along some fractures. The orange-stained cataclasite occurs primarily in the central region of the fault core intercalated with the orange-black quartzose foliated cataclasite (Figures 1b and 2a). It is distinctive as it lacks any foliation. The orange color appears to result from the weathering out of iron oxide. It is relatively incohesive with a grain size <1 mm and no features or textures are recognizable.

3.1.7. Fault Rock Sequence

[20] The mylonites derived from Ryoke protoliths are consistently the earliest recognized fault rocks preserved. They are heterogeneously overprinted by the effects of increasingly pervasive brittle fracturing, which develop cataclasites and foliated ultracataclasites. The latter are localized initially along fractures aligned parallel to the MTL leading to a crude mesoscale foliation, which is augmented by a subparallel ultrafine-grained fabric. The development of injection veins and irregular folds points to the localized onset of cataclastic flow. With increased deformation, the ultracataclasites become dominant and lose cohesion to form flow-banded, locally injected foliated gouge. Episodic carbonate veining is associated with, and reworked by, every stage of cataclastic deformation and eventually becomes focused in the most intensely deformed foliated gouges.

[21] The unfoliated orange and gray-green cataclasites are problematic in terms of their relative age. There is no clear evidence to suggest that they derived from later reworking of foliated cataclasites at shallower depths. However, while gray-green cataclasite preserves only relict mylonitic textures, the incipient development of ultracataclasite seams suggests that they may represent regions of ?strain hardened cataclasite effectively “frozen in” and little affected by the later localization of shearing and development of foliated cataclasite and gouge in adjacent units.

[22] Finally, at least two later phases of brittle faulting significantly disrupt and interslice the preexisting fault rock units in the MTL core. Both events are associated with late carbonate and local sulphide mineralization.

3.2. Mineralogy and Microstructures

3.2.1. Ryoke Mylonites

[23] The mylonites derived from metamorphosed Ryoke psammites and pelites are composed of alternating domains with differing quartz-mica contents. The black bands visible in outcrop are composed predominantly of very fine grained (<0.05 mm) quartz (~60%) and mica (~40%) with no porphyroclasts (Figure 4j). The orange colored bands consist of a fine-grained (~0.05–0.1 mm) recrystallized quartz-rich matrix with ~20% white mica and chlorite (Figure 4i). The coarser-grained (up to 0.7 mm in length) white micas exhibit mica-fish consistent with sinistral shear (Figure 4j). Plagioclase and K-feldspar porphyroclasts (up to 1 mm in length) and fractured garnet porphyroclasts (~0.5 mm in length) are common within the quartz-rich layers (Figure 4i). The feldspars show strained and sweeping extinction patterns, deformation twins and slight asymmetry (Figures 4i–4j), indicating limited ductile sinistral shear deformation. Thin (<0.1 mm wide) shear zones lined with very finely comminuted white mica run parallel or at low angles to the mylonitic foliation and are often localized along compositional boundaries or the tails of wrapped porphyroclasts and mica fish (Figures 4i–4j). The deformation textures and stable mineralogy of quartz-albite-white mica-chlorite suggests that mylonitization occurred under (lower) greenschist-facies metamorphic conditions.

[24] Greenschist-facies mylonitic fabrics are well preserved also in the central parts of tonalite clasts within the quartzo-feldspathic foliated cataclasite (Figure 4k). Plagio-

Figure 4. (a) Plan view of orange-black quartzose foliated cataclasite. (b) Plan view of black bands forming closely spaced network of ultracataclasite localizing along centimeter-spaced fractures, which together with Riedel shears break down orange quartzose layers and clasts. (c) Plan view of centimeter-scale sinistral shear bands. (d) Folded injection seam of ultracataclasite across orange quartzose cataclasite, observed within loose block. (e) Section looking SW of centimeter-scale fold affecting ultracataclasite units. (f) Polished block of Anko gouge containing thin (<1 mm) carbonate veins and clasts of quartzose cataclasite (Qcat) and carbonate (Car). Asymmetric wrapping of foliation around clasts suggests sinistral shear. (g) Plan view of gouge adjacent to upright faults; note Fe-oxide net veining subparallel to foliation. (h) Section looking SW of cusped-lobate boundary between Ryoke and Sambagawa derived gouge, where black Sambagawa gouge has injected into the Ryoke-derived unit. (i) Ryoke mylonite derived from metamorphosed psammite and pelite; note feldspar (F'spar) and garnet (Gnt) porphyroclasts in fine-grained quartz (Qtz) and white mica (WM) matrix. (j) White mica fish and boundary between quartz-rich and quartz-poor domains; note also slivers of finely comminuted white mica. (k) Tonalitic mylonite clast within quartzo-feldspathic foliated cataclasite. (l) Quartzo-feldspathic cataclasite showing angular quartz and altered feldspar clasts. (m) Dense cluster of parallel to subparallel fractures lined with fine-grained ultracataclasite stained with Fe-oxide. (n) Protocataclasite (P-cat) and foliated ultracataclasite (U-cat) seam with pressure solution seams (PSS) developed at the margins. Note that Figures 4i to 4n are all thin sections with crossed polars.

clase and subordinate K-feldspar porphyroclasts up to 3 mm in length exhibit limited crystal plastic deformation (undulose and sweeping extinction) and are breaking down to fine-grained aggregates of quartz and white mica. The mylonitic foliation wrapping around these porphyroclasts is defined by recrystallized quartz and biotite (often >0.05 mm). The quartz shows evidence of subgrain rotation and grain boundary migration recrystallization, with ribbons up to 1 mm in length having developed. Finely comminuted biotite is often localized within very thin (<0.1 mm across) shear zones oriented subparallel or at low angles to the mylonitic foliation. Isolated examples of highly fractured garnet porphyroclasts (~0.7–1 mm in length) occur breaking down to biotite (Figure 4k). The local preservation of biotite as a stable synkinematic reaction product may indicate that the mylonites at least initially developed under midgreenschist facies metamorphic conditions.

3.2.2. Quartzo-Feldspathic Cataclasite and Foliated Cataclasite

[25] These rocks are predominantly protocataclasites composed of highly fractured clasts of quartz, albite, K-feldspar and calcite ~0.06–1.2 mm in length (e.g., Figures 4l, 5a, and 5b). The feldspars are altered typically to white mica along cleavage and fracture planes (Figure 5b). The matrix represents ~25% of the protocataclasite and consists of fine-grained (<0.5 mm) quartz, kaolinite, calcite, chlorite and a Fe-rich dolomitic carbonate (Figures 5a–5b). Many clasts comprising fragments of albite or quartz are net veined by calcite (Figure 5b) and may be reworked equivalents to the calcite veins observed crosscutting the mylonites. There is only very limited development of a foliation, defined by the weak alignment of chlorite grains.

[26] Up to 3 mm thick ultracataclasite bands (85–90% ~5–10 μm matrix) are defined in part by dense clusters of parallel to subparallel fractures lined with ultrafine-grained material stained with Fe-oxide (Figure 4m). The clasts (~10–100 μm in length) consist of quartz, albite (highly altered to white mica) and calcite and sit in a very fine grained (<5–10 μm) foliated matrix of chlorite (~10–15%) and apparently later Fe-rich dolomitic carbonate (70–75%), plus quartz, kaolin, white mica and Fe-oxide (Figures 5c and 5d). The foliation is defined primarily by an interconnected network of aligned and extremely fine grained (~10 μm in length) phyllosilicates (mainly chlorite, see Figure 5c), which form an interconnected network only within the finest-grained sections of the ultracataclasite. Chlorite also often forms beard-like overgrowths adjacent to angular clasts of quartz (Figure 5d). Pressure solution seams are developed locally within the finest grained sections of the cataclasite, especially at the margins of foliated ultracataclasite seams (Figure 4n). Much of the carbonate mineralization is Fe-rich dolomite and together with chlorite makes up most (70–75%) of the ultracataclasite matrix. As the calcite vein material that cuts quartz and feldspar clasts (Figure 5b) is clearly entrained as clasts, its precipitation predates the Fe-rich dolomite surrounding these clasts.

3.2.3. Orange-Black Quartzose Foliated Cataclasite and Gouge

[27] Relict textures comparable to those found in the quartzo-feldspathic mylonites are preserved locally in the orange colored quartzose layers. Recrystallized quartz

grains (~0.05–0.1 mm) wrap around fractured relics of feldspar porphyroclasts (<1 mm) that are now mostly altered to fine-grained aggregates of white mica and kaolin (Figure 6a). The rest of the cataclasite is composed of a matrix of quartz, kaolinite and flecks of white mica (~30 μm in length). The latter are aligned to define a weak foliation (Figure 6b). A possible source for the kaolin and white mica is the breakdown of feldspar.

[28] The injection veins of ultracataclasite observed in the field (e.g., Figure 4d) are predominantly composed of fine-grained (<10 μm) quartz, with minor Fe-oxide and carbonate, but little or no feldspar. These accumulations show slight contrast variations due to crystallographic preferred orientation (CPO). Clasts (up to ~0.1 mm) of the surrounding cataclasite are entrained within the quartz.

[29] The black bands in outcrop are composed of fine-grained (matrix ~5–10 μm) ultracataclasite. The foliation visible appears to be defined by the parallel arrangement of fractures and associated fine-grained cataclasite material. Carbonate mineralization is more extensive within these ultracataclasites (Figures 6c–6e).

[30] The orange-black foliated cataclasite contains three types of carbonate: calcite, Fe-rich dolomite and siderite (Figures 6d and 6g). Calcite appears to be the earliest phase, occurring within quartz clasts (Figure 6d). Subsequently, extensive precipitation of Fe-rich dolomite occurred along fractures and within the cataclasite matrix (Figures 6b and 6d). Weathering out of the oxidized iron has resulted in Fe staining responsible for the distinctive orange color (Figures 4g, 6a, and 6c). Fe-rich sideritic carbonate is often associated also with the Fe-rich dolomite (Figures 6d–6e), although its typical location toward the centers of mineralized fractures suggests that it developed slightly later than the dolomite. Both phases have a porous appearance and exhibit good rhombic crystal faces (Figure 6e), probably due to precipitation into fluid-filled cavities. This implies that precipitation occurred late in the fault rock development although some minor brittle fracturing of carbonate occurred postprecipitation. Finally, net veins of Fe-oxide cut across all observed cataclastic textures (Figure 6b).

[31] The orange-black foliated gouges adjacent to faults that dissect the section have higher carbonate contents (~85% compared to ~70% in the orange and black foliated cataclasite). In thin section, clasts of cataclasite, including the parallel arranged fractures and ultracataclasite, sit within a predominantly carbonate matrix (Figure 6f). Within the Fe-rich dolomite matrix angular clasts of quartz and albite up to 100 μm in length occur.

3.2.4. Gray-Green and Orange-Stained Cataclasites

[32] The majority of clasts within the gray-green cataclasite are plagioclase and K-feldspar. Clasts are subangular to angular and range from 0.1 to 0.6 mm in length (Figure 6h). The feldspar clasts are highly fractured and are breaking down to fine-grained white mica, but preserve earlier ductile deformation features (strained and sweeping extinction). The matrix consists of quartz, white mica, chlorite, calcite and opaques with grain sizes ≤ 0.05 mm. White mica and calcite accumulations both form within the matrix. There is little foliation development except in thin (<0.1 mm thick) isolated seams of dark ultracataclasite. In thin section, few textural relationships are preserved in the orange-stained cataclasites as they are heavily altered to fine-grained

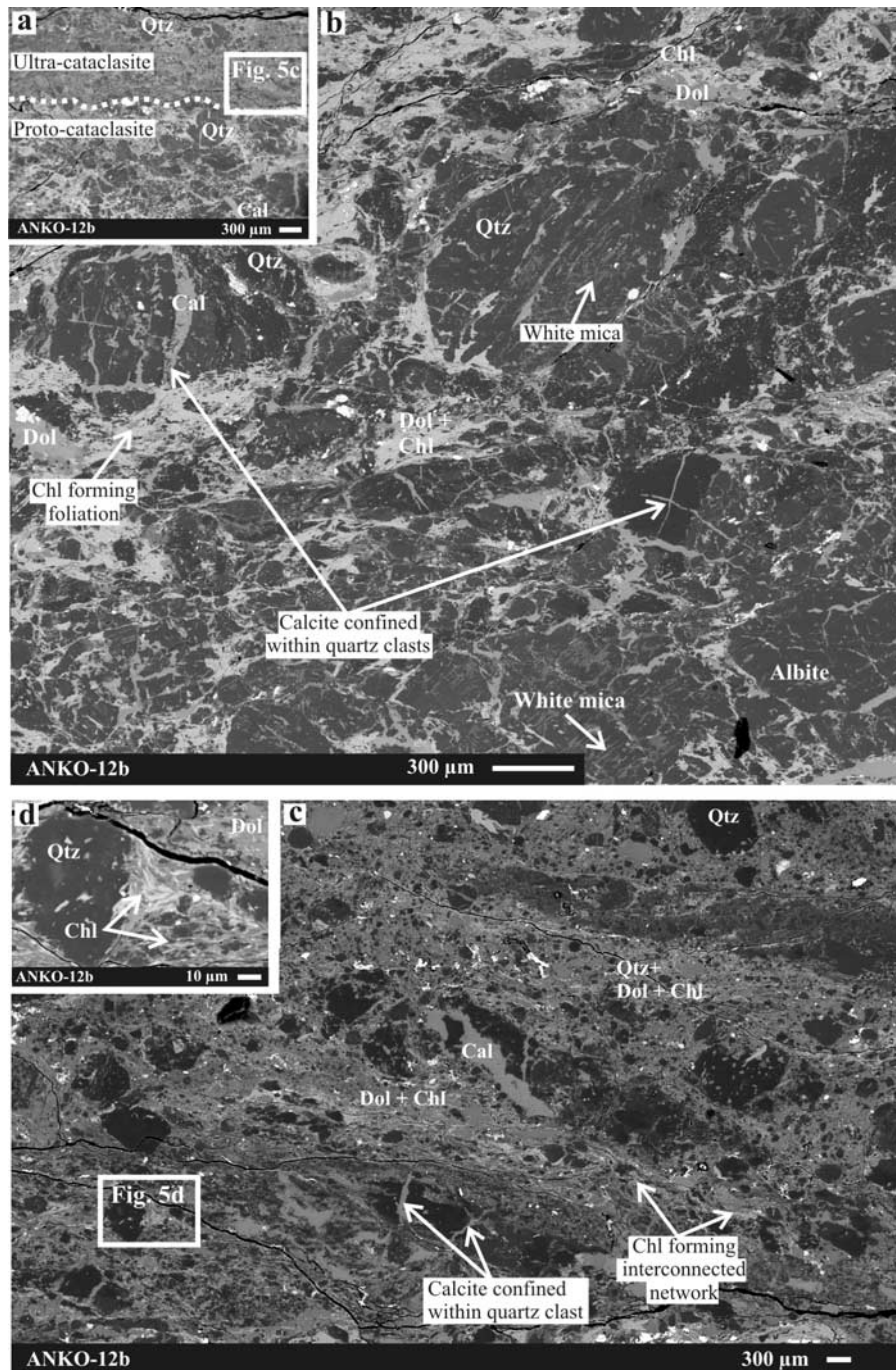


Figure 5. Backscattered electron SEM images of quartzo-feldspathic cataclasite and foliated cataclasite. (a) Boundary between protocataclasite and ultracataclasite. (b) Protocataclastic fault rock showing quartz (Qtz) and feldspar (F'spar) clasts containing early calcite in a matrix of quartz, kaolin (Ka), calcite (Cal), chlorite (Chl), and later Fe-rich dolomite (Dol). Limited foliation development is defined by alignment of chlorite grains. (c) Ultracataclastic fault rock containing quartz and feldspar clasts with a very fine grained matrix of Fe-rich dolomite and chlorite. Chlorite is defining a foliation and developing into an interconnected network. (d) Chlorite beard overgrowth on quartz clast.

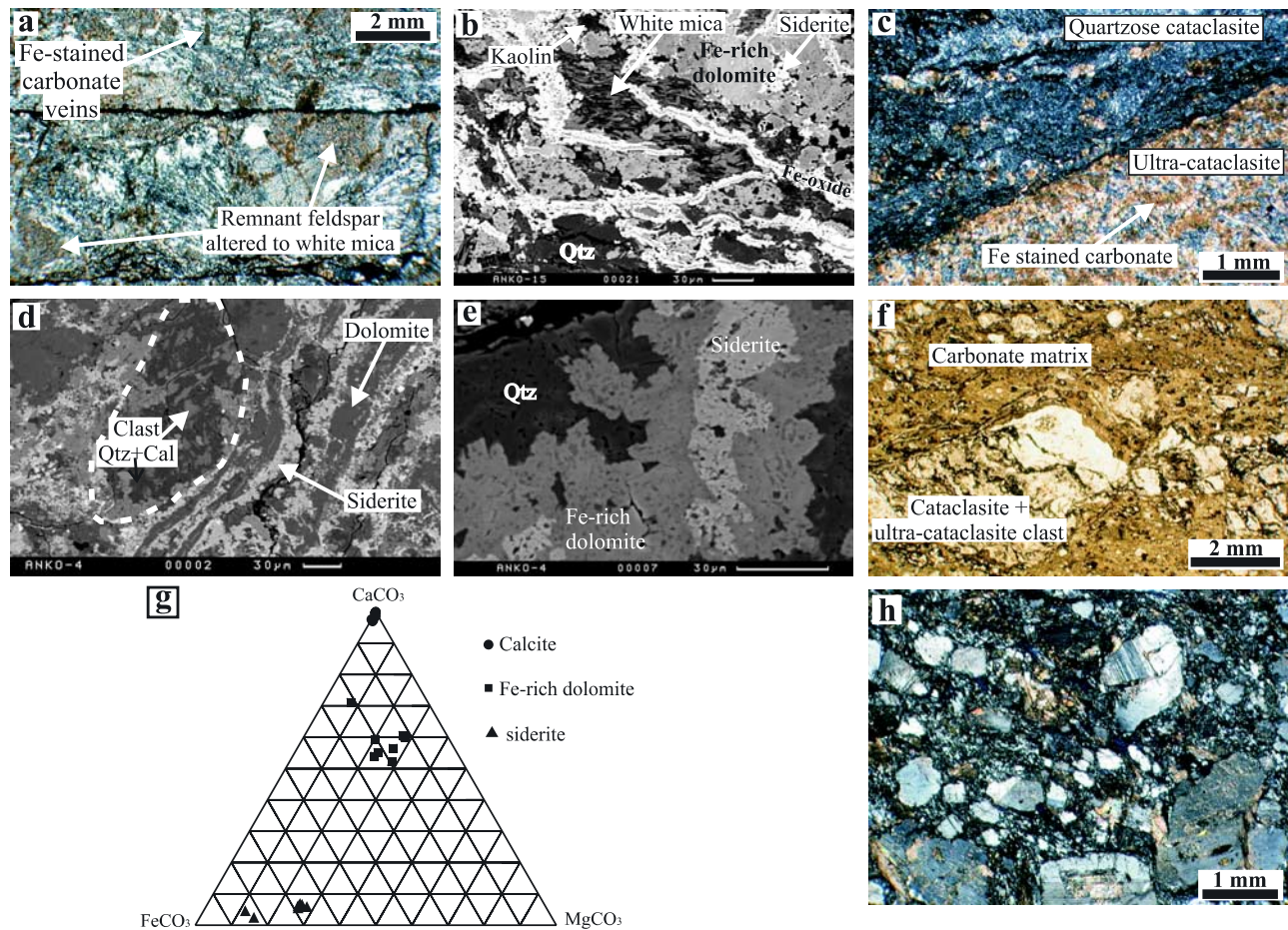


Figure 6. Microstructural observations of orange-black foliated cataclasite. (a) Plane polarized light thin section image of relict mylonitic textures. (b) Backscattered electron SEM image of aligned white mica and late net-veining Fe-oxide. (c) Cross polarized light thin section image of weathering out of oxidized iron within cataclasite. (d) Backscattered electron SEM image of three varieties of carbonate present. (e) Backscattered electron SEM image of rhombic and porous nature of late Fe-rich dolomite and siderite precipitation. (f) Plane polarized light thin section image of orange-black foliated gouge; note cataclasite clasts within a predominantly Fe-rich carbonate matrix. (g) Ternary phase diagram of comparative CaCO_3 – FeCO_3 – MgCO_3 content of carbonate within orange-black foliated cataclasites (data from microprobe analyses). (h) Thin section cross polarized light view of gray-green cataclasite showing highly fractured plagioclase and K-feldspar in fine-grained matrix of quartz, white mica, chlorite, calcite, and opaques; note feldspar breaking down to fine-grained white mica.

products (white mica and clay minerals) probably derived from the breakdown of feldspar.

4. Discussion

[33] Figure 7 presents a summary of the fault rock suites recognized in the core of the MTL in the Anko section, the interpreted deformation mechanism sequence and its inferred relationship to fluid influx, mineralogical changes and rheology.

4.1. Brittle Deformation, Fluid Flow, and the Development of Foliated Cataclasites

[34] The Anko section fault rocks indicate that the Ryoke metasedimentary and tonalitic protoliths were initially mylonitized during sinistral shear in a zone close to the MTL under middle to lower greenschist-facies pressure-

temperature conditions [cf. Hayama *et al.*, 1963; Hayama and Yamada, 1980; Takagi, 1986]. Exhumation to shallower depths and lower temperatures, that may or may not have occurred during the same prolonged phase of sinistral displacement, then led to reworking of the mylonites by brittle fracturing and cataclasis. The fractures are associated with the centimeter-scale development of Riedel-type brittle shears oriented at angles of up to 45° anticlockwise of the MTL. The formation of centimeter- to submillimeter-spaced fractures associated with faulting led to the development of a crude mesoscale foliation oriented parallel to the MTL. As explained below, this imposed an initial architectural hierarchy that fundamentally influenced the subsequent development of foliated cataclasite and gouge.

[35] Once each initial fracture had formed, other fractures localized adjacent to the break producing bands of densely spaced, subparallel fractures that eventually coalesced to

	Mylonitised tonalite	Mylonitised metasediment	Orange-stained cataclasite	Grey-green cataclasite	Quartz-felspar cataclasite & foliated cataclasite	Orange-black foliated cataclasite & gouge	Meso-scale faults	
							Upright strike-slip	Low angle reverse
Deformation sequence	1	1	2-?	2-?	2-3	3-4	2-5	6
Dominant deformation mechanisms	Crystal plasticity		Cataclasis		Cataclasis, fracture, frictional grain boundary sliding, cataclastic flow		Fracture & frictional sliding	
Fluid flux & mineralisation	Early calcite veins				Fe-rich dolomite precipitation		Hydrothermal alteration & carbonate precipitation	Minor sulphide mineralisation
				Siderite in open fractures				
				Fe oxide				
Rheology				Rheology dominated by interconnected network of ultra-fine fault rock				
			Reaction softening (feldspar breakdown)		Weakening due to onset of DMT			
			Periodic cyclic fluid overpressuring					

Figure 7. Summary of fault rock suites recognized in MTL core from the Anko Section and interpreted deformation mechanism sequence and its relationship to fluid influx, mineralogical changes, and rheological implications. DMT, diffusive mass transfer.

form submillimeter-scale seams of dark ultracataclasite (e.g., Figure 4m). These seams are found in all foliated cataclasites. They broaden by the progressive abrasion of wall rocks but rarely attain thicknesses of more than a few millimeters. The onset of brittle deformation coincides with significant fluid influx due to grain-scale dilatancy associated with cataclasis. The presence of an active fluid phase is indicated by (1) development of early calcite veins and mineralized breccias in fractured mylonite and protocataclasite; (2) ubiquitous breakdown of feldspar, biotite and garnet to fine-grained aggregates of phyllosilicates (white mica, chlorite); and (3) precipitation in ultracataclasites of fibrous chlorite as aligned overgrowths on clasts and matrix grains, leading to the rapid development of a foliation defined by an interconnected network of aligned phyllosilicate aggregates (e.g., Figures 5b–5c). The preferential localization of chlorite precipitation within ultracataclasites was promoted initially by their ultrafine grain size, which favors both chemical reaction and diffusive mass transfer (DMT) on the grain scale and hence the limited development of pressure solution seams (e.g., Figure 4n).

[36] In this way, the development of the initial fault network seems to have led to the establishment of two distinct textural domains with very different deformation behaviors in the MTL foliated cataclasites. The most intense deformation, and therefore largest displacements, are localized into a narrow, interconnected network of foliated ultracataclasites that enclose tens of-meters to millimeter-scale lenticular regions of less deformed protocataclasite (Figures 8a and 8b). In the protocataclasite regions (Figure 8c), grain-scale processes were dominated by frac-

ture, rigid rotation of grain fragments and presumably limited frictional sliding. In contrast, the grain-scale deformation mechanisms dominant in the foliated ultracataclasites (Figure 8d) involved significant amounts of fluid-assisted DMT, including grain boundary sliding and pressure solution.

[37] Most of the later carbonate and Fe-oxide mineralization is preferentially sited within foliated ultracataclasites and gouge, especially the orange-black quartzose foliated cataclasites of the MTL core. This may reflect channeling of fluid flow within the foliated and fracture-bound network of ultracataclasites (Figure 8a) or perhaps simply the high surface area available for reaction/precipitation in the ultra-fine cataclasites.

4.2. Evidence for Strain Weakening

[38] During frictional and viscous deformations, fault rock rheology depends upon the relative proportions of weak and strong phases and the connectivity of the weak phase [e.g., *Handy*, 1990, 1994]. The textures of the lower strain protocataclasite regions (e.g., Figure 8c) are likely representative of the fault zone as a whole in the first increments of deformation following exhumation. Fractured clasts of mylonite and calcite vein/mineral cements are randomly distributed and lie in direct contact with each other, forming a relatively strong load-bearing framework.

[39] Two lines of evidence suggest that the subsequent development of foliated ultracataclasite strands aligned subparallel to the MTL led to significant weakening.

[40] 1. Once established, much of the subsequent deformation (=displacement) localized preferentially into regions of foliated ultracataclasite, leading to the develop-

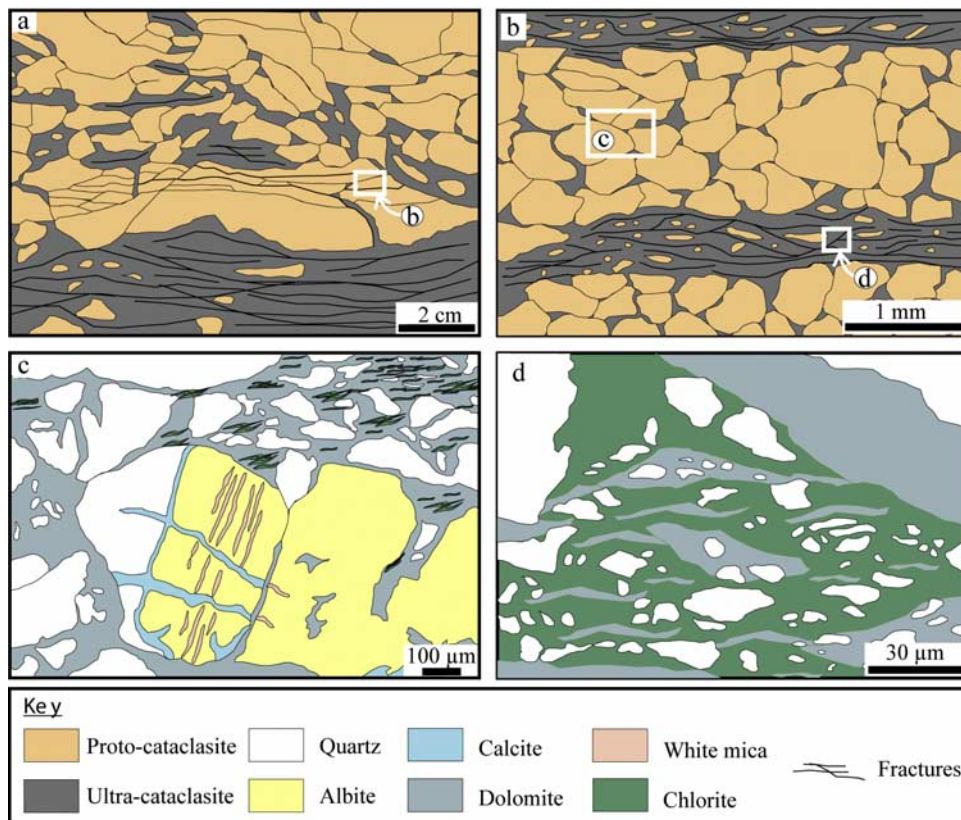


Figure 8. Schematic diagram depicting principal features of the Anko foliated cataclasite on various scales. (a) Hand-specimen scale showing regions of orange colored protocataclasite breaking down by subparallel fractures and regions of black colored ultracataclasite showing development of a crude foliation to give the overall cataclasite a banded appearance (see Figures 4a and 4b). (b) Thin section scale showing narrow black bands of closely spaced fractures around which ultracataclasite develops. Protocataclastic portions are clast supported and within ultracataclasite sections fractures and associated fine-grained material create an interlinked network (see Figure 4m). (c) Micron-scale view of protocataclasite showing clasts of quartz and albite within a matrix of dolomite with isolated patches of aligned chlorite growth (see Figure 5b). (d) Micron-scale view of ultracataclasite. Aligned chlorite development is more pervasive with evidence for limited DMT (e.g., chlorite forming beard like overgrowths adjacent to clasts). Aligned chlorite grains form an interconnected layer throughout the ultracataclasite. Note that the interlinked nature of foliated ultracataclasite on all scales makes it likely that the rheology of this fault rock dominated the overall behavior of the fault zone.

ment of flow-banded foliated gouges adjacent to major faulted boundaries (e.g., Figures 4c, 4f, and 4g), including the main Ryoike-Sambagawa contacts. The local development of folds (Figure 4e) and injection of mobilized units of ultracataclasite and gouge into adjacent rock units (Figure 4h) is similarly consistent with weakening.

[41] 2. The foliated ultracataclasites alone display evidence of fluid assisted DMT processes on grain scales and the development of an ultrafine-grained interconnected network of strongly aligned phyllosilicates (e.g., Figures 3, 4, and 5c). There is abundant evidence from both experimental studies [e.g., *Mares and Kronenberg*, 1993; *Bos and Spiers*, 2000, 2002; *Bos et al.*, 2000a, 2000b] and natural phyllosilicate-bearing fault rocks [e.g., *Wintsch et al.*, 1995; *Stewart et al.*, 2000; *Imber et al.*, 2001; *Collettini and Holdsworth*, 2004] that the establishment of interconnected phyllosilicate layers coupled with the onset of DMT leads to a profound reduction of long-term (steady state) strength. A more general reaction softening effect is likely also due to the

replacement of strong framework silicates by weak phyllosilicates [cf. *Gueydan et al.*, 2003], illustrated by the folding of crosscutting ultracataclasite seams within foliated cataclasites (e.g., Figures 4d–4e).

[42] In addition to the strain weakening effects, the consistent association of cataclasis and (mainly carbonate) mineralization suggests periodic development of high pore fluid pressures in the fault core, which would also likely lead to weakening, although on shorter timescales.

4.3. Fault Zone Rheology and Crustal Strength

[43] While brittle processes clearly played a key role in the formation and initial localization of the foliated ultracataclasite bands, the above mentioned evidence for weakening through interconnected phyllosilicate foliation development and diffusive mass transfer suggest that ultimately it is this that controlled the longer term strength of the fault core. The grain-scale overgrowth and pressure dissolution features widely observed in the foliated ultra-

cataclasites bear a striking resemblance to the microstructures produced in the experiments on analogue fault rocks reported by *Bos and Spiers* [2000, 2002; see also *Bos et al.*, 2000a, 2000b]. On this basis, we propose that strain weakening and long-term (steady state) strength of the cataclasite bands, and hence fault core, was controlled by the grain-scale mechanisms inferred to operate in the experimental examples, namely, a transition from initial cataclasis to slip on the developing phyllosilicate foliation with accommodation by cataclastic refinement and pressure solution of the intervening clasts.

[44] *Bos and Spiers* [2000, 2002] developed a microphysical model (Bos-Spiers model) that explained the steady state (large strain) slip behavior seen in their simulated fault experiments and applied this to predict the long-term strength of quartz-mica fault rocks under middle to upper crustal conditions [*Bos and Spiers*, 2002; see also *Niemeijer and Spiers*, 2005]. We adopt this model (Figures 9a–9c) in order to estimate the maximum weakening likely to be associated with the development of foliated cataclasites in the core of crustal faults such as the MTL. In the Bos-Spiers model, deformation of the foliated quartz-phyllosilicate fault rock (e.g., 20 vol % muscovite or chlorite) occurs by frictional slip within the phyllosilicate foliation, with accommodation at geometric undulations by pressure solution of the intervening grains and/or dilatational cataclasis (Figures 9a and 9b). For a matrix with a typical lognormal grain size distribution, the strength of the bulk material can be represented by the mechanical analogue and corresponding equations given in Figure 9c [see *Niemeijer and Spiers*, 2005].

[45] The model predicts that when sliding rates are high or temperatures low, diffusive mass transfer (pressure solution) is too slow to accommodate slip, so that dilatational/cataclastic disruption of the microstructure dominates, producing Byerlee-type frictional behavior (friction coefficient $\mu = 0.6–0.9$). *Niemeijer and Spiers* [2005] recently showed that this regime exhibits marked velocity weakening, in the terminology of the “rate and state friction” or RSF theory of fault slip [*Dieterich*, 1979], and is therefore potentially seismogenic. At lower sliding velocities or higher temperatures, diffusive mass transfer (pressure solution) in the matrix becomes rapid enough to accommodate slip on the irregular foliation without dilatation, and the shear strength decreases to values determined by the stress needed to drive frictional slip on the phyllosilicate foliation plus the necessary pressure solution (Figures 9b–9c). At still lower velocities or higher temperatures, pressure solution becomes so easy that fault rock strength is controlled mainly by the resistance to frictional slip on the foliation, which is expected to be relatively low (friction coefficient $\mu = 0.2–0.3$). In these two latter regimes, where pressure solution is an effective accommodation mechanism, a composite “frictional-viscous” fault rock rheology is predicted [*Bos et al.*, 2000b], whereby the shear resistance to sliding shows both a normal stress dependence, due to the resistance offered by frictional slip on the foliation, plus a shear rate dependence due to the viscous pressure solution component of deformation. In contrast to the dilatational/cataclastic regime, frictional-viscous sliding is velocity strengthening in the terminology of RSF theory, and therefore stable or nonseismogenic [*Niemeijer and Spiers*, 2005].

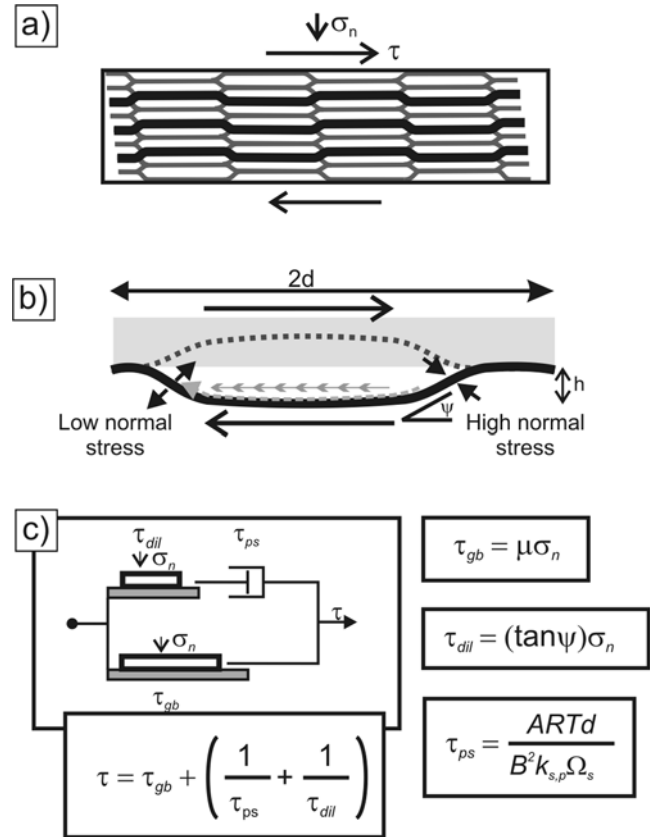


Figure 9. Elements of the microphysical model of *Bos and Spiers* [2002] for the rheological behavior of a foliated phyllosilicate bearing fault rock. (a) Schematic diagram of the model microstructure proposed by *Bos and Spiers* [2002], showing contiguous, anastomosing network of phyllosilicates surrounding elongate grains of a soluble solid (e.g., quartz). The shear strength of the fault rock is determined by the combined resistance to shear offered by frictional sliding on the phyllosilicate foliae, pressure solution in the soluble solid and dilatation on the foliation (work against the normal stress). (b) Schematic drawing of representative grain element of matrix, showing an active sliding surface in black. Shear sense is dextral. The diffusive mass flux from source to sink regions is indicated by a dashed arrow. The foliation waves have amplitude h , the grains have long axis d . The leading edge of the grain is inclined at angle ψ to the horizontal [after *Bos and Spiers*, 2002]. (c) Mechanical analogue diagram for shear deformation of the model microstructure, assuming zero porosity. The parameter τ_{gb} is the shear strength contribution offered by frictional sliding on the phyllosilicate foliae (friction coefficient μ), τ_{ps} is the shear strength contribution offered by pressure solution of the soluble matrix grains, τ_{dil} is the shear strength contribution offered by dilatation on the foliation (work against the normal stress via microstructural dilatation angle ψ), and σ_n is the normal stress. In the expression used to model pressure solution, A is a geometric constant of order unity, B is the matrix grain aspect ratio (taken as 5), d is the grain size (taken as $30 \mu\text{m}$), Ω_s is the molar volume of the soluble matrix phase, and $k_{s,p}$ is the phenomenological rate coefficient for dissolution (subscript s) or precipitation (p).

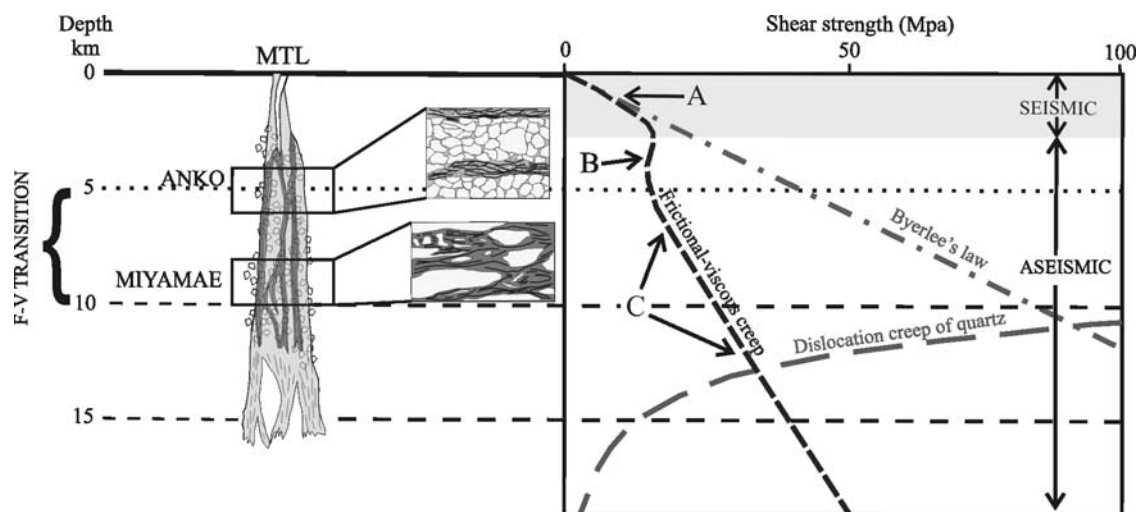


Figure 10. (left) Fault profile showing relative depths of formation and schematic textural diagrams of foliated cataclasite and gouge from Anko, Nagano Prefecture, and phyllonite from Miyamae, Mie Prefecture. (right) Corresponding strength-depth profiles for this section of the crust, assuming a strike slip fault, a geotherm of 25 K km^{-1} and a hydrostatic gradient of pore fluid pressure. A traditional two-mechanism fault strength versus depth profile is defined by Byerlee's law ($\mu = 0.75$) and a dislocation creep law for wet quartz [Luan and Paterson, 1992] and is drawn assuming an average fault zone strain rate of 10^{-12} s^{-1} . Also shown is the profile A–C predicted using the microphysical model of Bos and Spiers [2000, 2002] [see also Niemeijer and Spiers, 2005] describing the rheology of foliated phyllosilicate-rich fault rocks within the core of a crustal-scale fault zone (see Figure 9). For constructing this profile, a further strain rate enhancement to 10^{-10} s^{-1} is assumed, to account for the narrow dimensions of the fault core. The profile was constructed assuming a mean matrix grain size of $30 \mu\text{m}$ and microstructural parameters appropriate for a phyllosilicate content of 20% and a friction coefficient of 0.3. Portions A–C of the Bos-Spiers strength profile correspond to the following dominant processes: A, dilatation/cataclasis; B, pressure solution accommodated slip on the phyllosilicate foliation, with pressure solution controlling strength; C, pressure solution accommodated slip on the phyllosilicate foliation, with phyllosilicate friction coefficient controlling strength.

[46] Applying the model to a strike slip fault zone similar to the MTL or San Andreas Fault, and assuming microstructural parameters appropriate for a quartz-mica fault rock with a matrix grain size of $30 \mu\text{m}$ and 20% mica ($\mu = 0.25$), we predict a steady state strength profile of the type shown in Figure 10. The upper portion (A) of the profile represents the low-temperature (velocity weakening or potentially seismogenic) regime described above, in which dilatational cataclastic flow dominates. This is characterized by Byerlee-type frictional behavior ($\mu = 0.75$) and an increase in strength up to a depth of around 2.5 km. At depths in the range 2 to 5 km, portion (B) of the profile shows weakening of the fault rock with depth, as accommodation of slip on the foliation becomes easier due to thermal activation of pressure solution. At depths beyond 5 km, the model predicts increasing strength with depth (portion C of the profile), as pressure solution becomes so easy that frictional sliding on the foliation becomes strength determining with $\mu = 0.25$. Note that portions B and C of the profile correspond to velocity strengthening, hence aseismic, frictional-viscous slip behavior. Microstructural predictions implied by the model are that portion A will be characterized by cataclastic microstructures, portion B by a transition to foliated cataclasites with increasing evidence for matrix flow by diffusive mass transfer, and portion C by highly foliated, ductile-looking phyllonites [Niemeijer and Spiers, 2005].

[47] Compared to a conventional crustal fault strength profile constructed using Byerlee's law to describe frictional slip in the upper crust, plus a dislocation creep law for wet quartz to describe the transition to plastic flow in the midcrust (Figure 10), the model predicts a 30–70% reduction in steady state strength at midcrustal levels, i.e., in the 4–12 km depth range. It also predicts a thinning of the seismogenic zone to $<5 \text{ km}$ in a mature fault free of geometric asperities [Niemeijer and Spiers, 2005]. These effects are due to the onset at depths $>3 \text{ km}$ of frictional-viscous flow resulting from the combined effects of pressure solution and slip on the phyllosilicate foliation. If thermally activated crystal plastic or diffusional flow of the phyllosilicate phase is taken into account, the weakening predicted by the model would be even greater beyond 7–10 km depth [Niemeijer and Spiers, 2005]. On the other hand, if the friction coefficient of phyllosilicates increases with temperature and strain, reaching values of 0.4–0.5 under midcrustal conditions [see Mariani *et al.*, 2006], the weakening effect predicted by the Bos-Spiers model (Figure 10) may be reduced to perhaps 10–30%. Nonetheless, it seems reasonable to suppose that phyllosilicate production and the operation of solution transfer processes in crustal fault zones, as a result of initial cataclasis and fluid ingress, can be expected to produce significant weakening at depths of 3–10 km.

4.4. How Are Foliated Cataclasites/Gouges Related to Phyllonites?

[48] Foliated cataclastic fault rocks occur at a number of localities along the MTL (e.g., Tobe [Takagi *et al.*, 1992]; Hiruma (H. Takagi as cited by Snoke *et al.* [1998]); and Tsukide [Wibberley and Shimamoto, 2003]). Recently, Jefferies *et al.* [2006] suggested that the development of foliated cataclasites overprinting cataclastic fault rocks elsewhere in the MTL ultimately leads to the development of phyllonites because cataclasis in the vicinity of brittle fractures creates permeable pathways for the ingress of chemically active fluids into the fault zone. They describe evidence for fluid-assisted reactions in which load-bearing phases (e.g., feldspars) are replaced by fine-grained, foliated aggregates of weaker phyllosilicate minerals. However, the extent of this alteration and the precipitation of new minerals are far greater compared to the Anko section, leading to the formation of phyllonite bands at least 15 m thick. There is more evidence also for the operation of fluid-assisted, grain size-sensitive DMT processes, especially pressure solution, throughout the phyllonite. Nevertheless, comparison with experimental studies [e.g., Bos and Spiers, 2000, 2002], led Jefferies *et al.* [2006] to conclude similarly that the development of phyllonite could lead to the long-term weakening of the MTL and other crustal-scale faults as discussed here.

[49] We propose that the absence of phyllonite in the Anko section of the MTL compared to the section described by Jefferies *et al.* [2006] occurs because it is a less deeply exhumed section. The two sections therefore preserve fault rock assemblages that formed at different depths along the same fault at more or less the same time (Figure 10). This is supported by the observation that cataclastic rocks in both sections are associated with sinistral shearing events that overprint and rework preexisting mylonite-ultramylonite sequences. Thus, although the textural sequences and mineralogical development of the phyllosilicate-bearing fault rocks are similar, the finer phyllosilicate grain sizes and the lesser importance of pressure solution and reaction softening at Anko is consistent with a shallower crustal location.

5. Conclusions

[50] Examination of the MTL fault core exposed at Anko shows that the development of an interconnected centimeter- to submillimeter-scale network of coalescing fractures and associated ultrafine-grained cataclasite plays a major role in controlling where shear localization and weakening occur. Deformation mechanisms within the developing cataclasites and foliated cataclasites are dominated by fracture, frictional grain boundary sliding and cataclastic flow. Fluid influx initially occurred during the onset of cataclasis and led to a switch in dominant deformation mechanisms within the finest-grained sections of ultracataclasite formed around the preexisting fracture network to fluid-assisted reaction softening and diffusive mass transfer (pressure solution) processes. These aided the development of a foliation defined by the alignment phyllosilicate (chlorite), with further chlorite growth leading to the creation of an interlinked network within the matrix and ultracataclasite strands in the foliated cataclasite. The pattern of initial fracture development provided the architecture for the

creation of interlinked zones of fine-grained weak material throughout the fault core, which dramatically altered the rheology of the fault core.

[51] On textural and mineralogical grounds, the development of foliated cataclasite and phyllonite along the MTL are equivalent in both space (depth) and time (Figure 10). These observations are consistent with recent microphysical models [i.e., Bos and Spiers, 2000, 2002], which suggest that the formation of foliated cataclasites and phyllonites within the core of large crustal-scale fault zones can dramatically reduce the long-term or steady state fault zone strength, effectively reducing the thickness of seismogenic layer to <5 km (Figure 10). On shorter timescales, the fracture bound network of foliated ultracataclasite and gouges likely acted as effective fluid seals leading to periodic overpressuring, as indicated by the widespread (mainly carbonate) mineralization in the core of the MTL. These findings have important implications for the weakening of crustal-scale faults in many tectonic settings worldwide.

[52] **Acknowledgments.** S.J. acknowledges receipt of a NERC studentship (NER/S/A/2001/06126) and REH funding from the Royal Society. E. Condliffe, N. Marsh, and R. Kelly provided invaluable help and support during SEM and analytical work. Finally, we thank F. Gueydan, N. Mancktelow, and G. Rosenbaum for their very constructive and detailed comments as reviewers.

References

- Beeler, N. M., T. E. Tullis, M. L. Blanpied, and J. D. Weeks (1996), Frictional behavior of large displacement experimental faults, *J. Geophys. Res.*, *101*, 8697–8715.
- Bos, B., and C. J. Spiers (2000), Effect of phyllosilicates on fluid-assisted healing of gouge-bearing faults, *Earth Planet. Sci. Lett.*, *184*, 199–210.
- Bos, B., and C. J. Spiers (2002), Frictional-viscous flow of phyllosilicate-bearing fault rock: Microphysical model and implications for crustal strength profiles, *J. Geophys. Res.*, *107*(B2), 2028, doi:10.1029/2001JB000301.
- Bos, B., C. J. Peach, and C. J. Spiers (2000a), Slip behavior of simulated gouge-bearing faults under conditions favoring pressure solution, *J. Geophys. Res.*, *105*, 16,699–16,717.
- Bos, B., C. J. Peach, and C. J. Spiers (2000b), Frictional-viscous flow of simulated fault gouge caused by the combined effects of phyllosilicates and pressure solution, *Tectonophysics*, *327*, 173–194.
- Chester, F. M. (1995), A rheologic model for wet crust applied to strike-slip faults, *J. Geophys. Res.*, *100*, 13,033–13,044.
- Chester, F. M., and J. M. Logan (1986), Implications for mechanical properties of brittle faults from observations of the Punchbowl Fault Zone, California, *Pure Appl. Geophys.*, *124*, 79–106.
- Chester, F. M., M. Friedman, and J. M. Logan (1985), Foliated cataclasites, *Tectonophysics*, *111*, 139–146.
- Chester, F. M., J. P. Evans, and R. L. Biegel (1993), Internal structure and weakening mechanisms of the San Andreas fault, *J. Geophys. Res.*, *98*, 771–786.
- Collettini, C., and R. E. Holdsworth (2004), Fault zone weakening and character of slip along low-angle normal faults: Insights from the Zuccale Fault, Elba, Italy, *J. Geol. Soc. London*, *161*, 1039–1051.
- Dieterich, J. H. (1979), Modeling of rock friction: 1. Experimental results and constitutive equations, *J. Geophys. Res.*, *84*, 2162–2168.
- Evans, J. P., and F. M. Chester (1995), Fluid-rock interaction in faults of the San Andreas system: Inferences from San Gabriel fault rock geochemistry and microstructures, *J. Geophys. Res.*, *100*, 13,007–13,020.
- Gueydan, F., Y. M. Leroy, L. Jolivet, and P. Agard (2003), Analysis of continental midcrustal strain localization induced by microfracturing and reaction-softening, *J. Geophys. Res.*, *108*(B2), 2064, doi:10.1029/2001JB000611.
- Handy, M. R. (1990), The solid-state flow of polymineralic rocks, *J. Geophys. Res.*, *95*, 8647–8661.
- Handy, M. R. (1994), Flow laws for rocks containing two non-linear viscous phases: A phenomenological approach, *J. Struct. Geol.*, *16*, 287–301.

- Hara, I., K. Shyoji, Y. Sakurai, S. Yokoyama, and K. Hide (1980), Origin of the Median Tectonic Line and its initial shape, *Mem. Geol. Soc. Jpn.*, *18*, 27–49.
- Hayama, Y., and T. Yamada (1980), Median Tectonic Line at the stage of its origin in relation to plutonism and mylonitisation in the Ryoke Belt, *Mem. Geol. Soc. Jpn.*, *18*, 5–26.
- Hayama, Y., K. Miyagawa, W. Nakajima, and T. Yamada (1963), The Kashio tectonic zone, Urakawa to Wada area, central Japan (in Japanese with English abstract), *Earth Sci.*, *66*, 23–31.
- Holdsworth, R. E. (2004), Weak faults—Rotten cores, *Science*, *303*, 181–182.
- Holdsworth, R. E., M. Stewart, J. Imber, and R. A. Strachan (2001), The structure and rheological evolution of reactivated continental fault zones: A review and case study, in *Continental Reactivation and Reworking*, edited by J. Miller et al., *Geol. Soc. Spec. Publ.*, *184*, 115–137.
- Ichikawa, K. (1980), Geohistory of the Median Tectonic Line of southwest Japan, *Mem. Geol. Surv. Jpn.*, *18*, 187–212.
- Imber, J., R. E. Holdsworth, C. A. Butler, and R. A. Strachan (2001), A reappraisal of the Sibson-Scholz fault zone model: The nature of the frictional to viscous (“brittle-ductile”) transition along a long-lived, crustal-scale fault, Outer Hebrides, Scotland, *Tectonics*, *20*, 601–624.
- Ito, M. (1978), Granitic rocks and mylonitisation in the Kayumi district, Mie Prefecture (in Japanese), *MTL*, *3*, 99–101.
- Jefferies, S. P., R. E. Holdsworth, C. A. J. Wibberley, T. Shimamoto, C. J. Spiers, A. J. Niemeijer, and G. E. Lloyd (2006), The nature and importance of phyllonite development in crustal-scale fault cores: An example from the Median Tectonic Line, Japan, *J. Struct. Geol.*, *28*, 220–235.
- Luan, F. C., and M. S. Paterson (1992), Preparation and deformation of synthetic aggregates of quartz, *J. Geophys. Res.*, *97*, 301–320.
- Mares, U. M., and A. K. Kronenberg (1993), Experimental deformation of muscovite, *J. Struct. Geol.*, *15*, 1061–1075.
- Mariani, E., K. H. Brodie, and E. H. Rutter (2006), Experimental deformation of muscovite shear zones at high temperature under hydrothermal conditions and the strength of phyllosilicate-bearing faults in nature, *J. Struct. Geol.*, *28*, 1569–1587.
- Niemeijer, A. R., and C. J. Spiers (2005), Influence of phyllosilicates on fault strength in the brittle-ductile transition: Insights from rock analogue experiments, in *High-Strain Zone: Structure and Physical Properties*, edited by D. Bruhn and L. Burlini, *Geol. Soc. Spec. Publ.*, *245*, 303–327.
- Ohtomo, Y. (1993), Origin of the Median Tectonic Line, *J. Sci. Hiroshima Univ.*, *9*, 611–669.
- Okada, A. (1980), Quaternary faulting along the Median Tectonic Line of southwest Japan, *Mem. Geol. Soc. Jpn.*, *18*, 79–108.
- Schmid, S. M., and M. R. Handy (1991), Towards a genetic classification of fault rocks: Geological usage and tectonophysical implications, in *Controversies in Modern Geology*, edited by D. W. Müller, J. A. McKenzie, and H. Weissert, pp. 339–361, Elsevier, New York.
- Sibson, R. H. (1977), Fault rocks and fault mechanisms, *J. Geol. Soc. London*, *133*, 191–213.
- Snoke, A. W., J. Tullis, and V. R. Todd (1998), *Fault-Related Rocks: A Photographic Atlas*, 613 pp., Princeton Univ. Press, Princeton, N. J.
- Stewart, M., R. E. Holdsworth, and R. A. Strachan (2000), Deformation processes and weakening mechanisms within the frictional-viscous transition zone of major crustal-scale faults: Insights from the Great Glen Fault Zone, Scotland, *J. Struct. Geol.*, *22*, 543–560.
- Suzuki, K., and M. Adachi (1998), Denudation history of the high T/P Ryoke metamorphic belt, southwest Japan: Constraints from CHIME monazite ages of gneisses and granitoids, *J. Meteorol. Geol.*, *16*, 23–37.
- Takagi, H. (1984), Mylonitic rocks along the Median Tectonic Line in Takato-Ichinose area, Nagano Prefecture (in Japanese with English abstract), *J. Geol. Soc. Jpn.*, *90*, 81–100.
- Takagi, H. (1986), Implications of mylonitic microstructures for the geotectonic evolution of the Median Tectonic Line, central Japan, *J. Struct. Geol.*, *8*, 3–14.
- Takagi, H., T. Takeshita, S. Uchiumi, and M. Inoue (1992), Middle Miocene normal faulting along the Tobe thrust in western Shikoku (in Japanese with English abstract), *J. Geol. Soc. Jpn.*, *98*, 1069–1072.
- Tanaka, H., H. Takagi, and M. Inoue (1996), Mode of cataclastic deformation and hydrothermal alteration of the fault rocks and history of fault activity along the Median Tectonic Line, central Japan (in Japanese with English abstract), *J. Tectonic Res. Group Jpn.*, *41*, 31–44.
- Wibberley, C. A. J. (2005), Initiation of basement thrust detachments by fault-zone reaction weakening, in *High-Strain Zone: Structure and Physical Properties*, edited by D. Bruhn and L. Burlini, *Geol. Soc. Spec. Publ.*, *245*, 347–372.
- Wibberley, C. A. J., and T. Shimamoto (2003), Internal structure and permeability of major-slip fault zones: The Median Tectonic Line in Mie Prefecture, southwest Japan, *J. Struct. Geol.*, *25*, 59–78.
- Wintsch, R. P., R. Christofferson, and A. K. Kronenberg (1995), Fluid-rock reaction weakening of fault zones, *J. Geophys. Res.*, *100*, 13,021–13,032.
- Yamamoto, H. (1994), Kinematics of mylonitic rocks along the Median Tectonic Line, Akaishi Range, central Japan, *J. Struct. Geol.*, *16*, 61–70.
- Yund, R. A., M. L. Blanfield, T. E. Tullis, and J. D. Weeks (1990), Amorphous material in high strain experimental fault gouges, *J. Geophys. Res.*, *95*, 15,589–15,602.

R. E. Holdsworth and S. P. Jefferies, Reactivation Research Group, Department of Earth Sciences, University of Durham, Durham DH1 3LE, UK. (r.e.holdsworth@durham.ac.uk)

G. E. Lloyd, Department of Earth Sciences, University of Leeds, Leeds LS2 9JT, UK.

T. Shimamoto, Department of Geology and Mineralogy, Graduate School of Science, Kyoto University, Kyoto 606-8501, Japan.

C. J. Spiers, HPT Laboratory, Department of Earth Sciences, Utrecht University, P.O. Box 80021, NL-3508 TA Utrecht, Netherlands.

H. Takagi, Department of Earth Science, Waseda University, 1-104 Totsumakachi, Shinjuku-ku, Tokyo, 169-8050, Japan.